INSTITUTE OF PLASMA PHYSICS

NAGOYA UNIVERSITY

RESEARCH REPORT

NAGOYA, JAPAN

TOKAMAK EXPERIMENTS ON JIPP T-II WITH PULSED GAS INJECTION

K. Toi, S. Itoh, J. Fujita, K. Kadota,
K. Kawahata, Y. Kawasumi, K. Matsuura,
N. Noda, S. Tanahashi

IPPJ-322 February 1978

Further communication about this report is to be sent to the Research Information Center, Institute of Plasma Physics, Nagoya University, Nagoya, Japan.

ABSTRACT

The confinement of tokamak plasma has been investigated in the wide range of electron density $\bar{n}_e$ from 1×10^{13} to 5×10^{13} cm^{-3} by using the pulsed gas injection. The gross energy confinement time $<\tau_E>$ increases with increase of electron density and reaches 14 msec. The averaged effective ionic charge derived from plasma conductivity $<Z_{eff}> \equiv <\sigma_{SP}/\sigma_{exp}>$ is about 1 to 2 in the regime of small streaming parameter ($<v_d/v_{the}> = 0.01 \sim 0.08$). The ratio of ion temperature to electron one is in the range greater than 0.5. This fact means that the ion energy confinement time is greater than the electron-ion energy relaxation time. Excessive injection of cold neutral gas excites m = 2 MHD oscillations. Much more gas injection leads to the remarkable cooling of plasma periphery and disruptive instabilities. These MHD oscillations and disruptive instabilities have been suppressed by the heating of plasma periphery with the second rapid rise of plasma current.

1. INTRODUCTION

In most tokamak discharges by the static gas feed, the electron density reaches the peak value corresponding to the filling pressure within several milliseconds and decreases continuously. In the final phase of discharge the intense hard X-ray emission often appears because of decrease of electron density. Even if the filling pressure is increased, the electron density does not increase in proportion to the filling pressure except for the first peak of electron density. The line-averaged electron density $\bar{n}_e$ is limited to about 3×10^{13} cm^{-3} in the quasi-steady state of discharge. The above-mentioned continuous decrease of electron density is overcome by the pulsed gas injection in the course of discharge and the electron density can be changed in the wide range. In JIPP T-II, $\bar{n}_e$ has been changed from 1×10^{13} to 5×10^{13} cm^{-3} by the pulsed gas injection though $\bar{n}_e$ is limited to about 2×10^{13} cm^{-3} in the static gas feed.

In this paper, plasma properties of JIPP T-II are investigated in both comparatively low and high density regimes. Firstly, the central electron and ion temperatures (T_{e0} and T_{i0}), $\langle \sigma_{SP}/\sigma_{exp} \rangle$, T_{i0}/T_{e0} and energy confinement time $\langle \tau_E \rangle$ are shown as functions of the plasma parameters. Secondly, temporal evolutions of the plasma parameters are also shown for two types of discharges in the much gas injection. Lastly, we have tried the suppression of disruptive instabilities due to the intense gas injection by the second rapid rise of plasma current which is applied in appropriate timing with the gas injection. The effectiveness of heating of plasma periphery to suppress the disruptive instability is demonstrated.

2. EXPERIMENTAL ARRANGEMENTS

In this section the JIPP T-II device and diagnostic instruments are briefly described. The JIPP T-II is a hybrid device of tokamak and stellarator with resistive shell (Fig.1)[1].

The specifications of the JIPP T-II device including various power supplies and vacuum system are summarized in Table 1. The hydrogen gas purified through the palladium foil is fed steadily and pulsively by using the piezo-electric valves through the tangential port (Fig.2). Usually the initial filling pressure P_{fl} is 1.2×10^{-4} to 3.0×10^{-4} Torr H_2, and additional gas is pulsively injected in the course of discharge. The electron density measured on the opposite side of the gas filling port begins to increase within about 6 msec after applying voltage to piezo-electric crystals (Fig.3).

The discharge cleaning is not carried out, but the most of the data are obtained after about twenty shots of 120 kA discharge to determine the experimental conditions. By these discharges the wall conditions are in equilibrium state for the neutral gas balance, and the reproducibility becomes very well.

The positions of diagnostic instruments are shown in Fig.2. The diagnostic instruments are as follows: Thomson scattering for electron temperature and density; fast neutral energy analyzer for ion temperature; 4 mm microwave interferometer for electron density; visible light spectroscopy for the H_α and impurity line intensities, and ion temperature by Doppler broadening; NaI scintillator for hard X-ray emission; and some kinds of magnetic loops and probes for plasma current, loop voltage, and plasma positions and MHD oscillations. The image of H_α light over the plasma cross section at the limiter is always monitored

by the TV camera through the tangential port. Soft X-ray measurements by liquid N_2 cooled Si(Li) diode and multichannel PIN diodes are in adjustment. VUV spectrometer, and 2 mm microwave and far infra-red laser interferometer are in preparation.

3. FEEDBACK CONTROL OF PLASMA POSITION

The JIPP T-II device has no conducting shell but has only the resistive shell with the skin time of 5.2 msec for the vertical field. Therefore, it is important to control the plasma in the optimum position. The horizontal position is feedback-controlled by the resultant vertical field of the stationary field (B_{vd}) and the negative one which is controlled by a digital mini-computer (B_{vf}). The required vertical field is estimated by the mini-computer in accordance with the Mukhovatov and Shafranov equation[2].

In the experiments during the summer of 1976[1], the feedback control loop was in the marginal state and the plasma position fluctuated with the amplitude of about 2 cm. The gain parameters in the computer program to be in stable state were determined by the stability analysis including the program of the digital computer[3]. The results of the analysis agree well with the feedback control experiment. The adjustment of the loop gain is carried out by the change of the gain value of computer calculation (K_g). However, plasma position deviates from the desirable one since the effective reference input resulted from $K_g < 1$ is proportional to $A_1(1 - 1/K_g)\cdot(B_{vd} - A_2 I_p)$, where A_1 and A_2 are the given parameters. Therefore, the horizontal displacement is not maintained in the constant and most desirable value with time. In this situation the good tokamak plasma can be obtained by adjusting the

parameters A_1 and A_2 to a certain extent.

The power supply and coils are now under reconstruction in order that the feedback control of plasma position should be carried out more accurately. The vertical field will be produced by one sort of coil and feedback-controlled from the beginning of the discharge.

The vertical position of plasma is also feedback-controlled by horizontal field coil driven by transistor power supply.

4. PLASMA CONFINEMENT IN THE JIPP T-II

In this section we describe electron and ion temperatures as functions of the various plasma parameters. The plasma conductivity is compared with the Spitzer's one and the averaged effective ionic charge is estimated. The ratio of ion temperature to electron one is discussed by considering the energy balance of electrons.

The experiments have been carried out in the following discharge conditions; toroidal field B_t = 15 $\sim$ 30 kG, peak plasma current I_p = 60 $\sim$ 160 kA, maximum aperture radius of limiter a_L = 17 cm, safety factor at the plasma surface $q(a)$ = 2 $\sim$ 6 and initial filling gas pressure $P_{fl} = 1.2 \times 10^{-4} \sim 3.0 \times 10^{-4}$ Torr H_2. The main plasma parameters obtained under the above conditions are T_{e0} = 400 $\sim$ 1300 eV, T_{i0} = 250 $\sim$ 720 eV and line-averaged density $\bar{n}_e = 1 \sim 5 \times 10^{13}$ cm^{-3}.

4.1 Electron Temperature

Electron temperatures are measured at the positions of r = -1.5 cm (inward), r = 2.4 cm (outward) and r = 6.2 cm (outward) by Thomson scattering. As the observation area is limited by the helical coil, it is difficult to obtain the profile of electron temperature accurately. However, we can predict the profile of the electron temperature to a

certain extent. For all discharges the profiles can be approximately expressed as bell-shape $T_e(x) = T_{e0}(1 - x^2)^n$, where n is the index to determine the profile shape. Figure 4 shows the relationship between central electron temperature and plasma current for the various electron densities. At the lower density regime T_{e0} increases with I_p^{α} ($0.8 < \alpha < 1$), but tends to saturate with I_p as density increases. This fact is caused from the shrinkage of effective plasma radius by the cold neutral injection. In the high density regime the higher q(a) is required to obtain the better confinement. The scattering of the data in Fig.4 may be caused from difference of q(a). The dependence of T_{e0}/I_p on q(a) is shown in Fig.5. Within the range of $q(a) = 2 \sim 6$, T_{e0} is proportional to $I_p q(a)^{1/2}$ for $\bar{n}_e \gtrsim 3 \times 10^{13}$ cm^{-3}. However, T_{e0} is nearly proportional to I_p in the lower density regime ($\bar{n}_e \lesssim 2.5 \times 10^{13}$ cm^{-3}), independent of q(a).

4.2 Ion Temperature

Ion temperature on a plamsa axis (T_{i0}) have been obtained from analysis of the energy spectra of fast neutral atoms emitted by charge exchange processes. The flux of fast neutral atoms are detected by the neutral particle energy analyzer of seven channels (NEA). The particles with energy of about 400 eV to 3 keV are counted every time interval of 10 msec and time variation of ion temperature is deduced. For the above experimental conditions, $T_{i0} = 250 \sim 720$ eV. It is a question whether ion temperature obtained from NEA viewing tangentially agrees with one by NEA viewing radially[4-6]. In tokamak plasma, the temperature of transit ion is usually higher than that of trapped ion [4,5]. The difference of them depends remarkably on the energy range of detected neutral atoms and the aspect ratio of plasma. The time required for trapped ion to escape from trapped state is estimated as $\tau_{mix} = \tau_{ii}(8a/\pi^2 R)$,

where τ_{ii} is the ion-ion collision time, a is the minor radius of plasma and R is the major radius [7]. Even if the particle energy is 3 keV for the lowest electron density, $\tau_{mix} \simeq 1.4$ msec. Therefore, the difference of temperatures between transit and trapped ions is very small in the quasi-steady state. From above discussion, it is concluded that the ion temperature obtained by NEA viewing tangentially is nearly equal to the one obtained by NEA viewing radially.

The ions of tokamak plasmas obtained in the experiments are mainly in the plateau regime of the neoclassical transport theory. We compare the ion temperature with the one predicted from the Artsimovich's scaling law in Fig.6. Both show the good agreement with each other.

4.3 Plasma Conductivity

The ratio of Spitzer's conductivity (σ_{SP}) estimated from electron temperature and density to the experimental one (σ_{exp}) can be often used as an easy evaluation of impurity contents in plasma. The value estimated from plasma conductivity may be nearly equal or less than unity in the discharge where the run-away electrons carry the considerable part of plasma current. In ALCATOR, it has been shown that this discharge regime can be determined by the averaged streaming parameter $\langle v_d/v_{the} \rangle$ [8,9]. According to these references, the critical value of streaming parameter is 0.4 for hydrogen plasma and then two-component electron distribution function is obtained. Moreover, RF emission at frequencies higher than and equal to the ion plasma frequency appears, and strong ion heating occurs. In JIPP T-II, the averaged streaming parameter is 0.01 to 0.08 for all experiments even if the uncertainty of electron temperature and density profiles is considered. The spectra of scattered light intensity are fit for the Gaussian profile very well.

It is concluded that JIPP T-II plasma is not in the slide-way regime

investigated in ALCATOR but in the collisional regime where Coulomb collisions are dominant process. The relation between $\langle\sigma_{SP}/\sigma_{exp}\rangle$ and the streaming parameter is shown in Fig.7. The spread of the experimental points is due to the uncertainty of the profiles. Here the profiles of electron temperature, electron density and current density are assumed as $T_e = T_{e0}(1 - x^2)^n$, $n_e = n_{e0}(1 - x^2)$ and $j \propto T_e^{3/2}$, respectively, where $n = 1 \sim 2$ for lower electron density and $n = 2 \sim 3$ for higher electron density according to the measurements by the Thomson scattering and microwave interferometer. The larger is shot number of discharge, the plasma of the lower $\langle\sigma_{SP}/\sigma_{exp}\rangle$ is obtained. From above description it is concluded that the averaged ionic charge of plasma is the considerably lower value of 1 to 2. This suggests that the content of impurities is in lower level though the informations of heavy impurities are not yet obtained. The lower $\langle Z_{eff}\rangle$ discharge is considered to be due to cleanness of vacuum chamber, high purity of filling gas and the use of the molybdenum limiter made by the electron-beam melting method.

4.4 Ratio of Ion Temperature to Electron Temperature

In the most discharges of JIPP T-II, T_{io}/T_{eo} is greater than 0.5. In this subsection this fact is discussed as follows. The thermal energy balance of the ohmically heated hydrogen plasma is determined by the following equations,

$$\frac{dW_e}{dt} + \frac{W_e}{\langle\tau_e\rangle} = P_{OH} - P_{ei} \ , \tag{4.1}$$

$$\frac{dW_i}{dt} + \frac{W_i}{\langle\tau_i\rangle} = P_{ei} \ , \tag{4.2}$$

$$P_{ei} = \frac{W_e - W_i}{\langle\tau_{eq}\rangle} \ , \tag{4.3}$$

where $\langle\tau_e\rangle$ and $\langle\tau_i\rangle$ are the effective electron and ion energy confinement

times, P_{OH} is the ohmic input power, and $<\tau_{eq}>$ is the electron-ion energy relaxation time. The temperature ratio T_{i0}/T_{e0} is directly determined by Eq.(4.2). In the quasi-steady state, Eq.(4.2) is reduced to

$$\frac{W_i}{W_e} \simeq \frac{1}{1 + <\tau_{eq}>/<\tau_i>} \quad . \tag{4.4}$$

When the profiles of electron and ion temperatures have the same shape in the hydrogen plasma with $<Z_{eff}> = 1 \sim 2$,

$$\frac{W_i}{W_e} = \frac{<n_p T_i>}{<n_e T_e>} \simeq \frac{T_{i0}}{T_{e0}} \quad . \tag{4.5}$$

Therefore,

$$\frac{T_{i0}}{T_{e0}} \simeq \frac{1}{1 + <\tau_{eq}>/<\tau_i>} \quad . \tag{4.6}$$

The result of $T_{i0}/T_{e0} \gtrsim 0.5$ means $<\tau_{eq}> \lesssim <\tau_i>$.

The ion energy confinement time is determined by thermal conduction ($<\tau_i>_{HC}$), particle diffusion ($<\tau_i>_{PD}$), and charge exchange ($<\tau_i>_{CX}$), i.e.,

$$\frac{1}{<\tau_i>} = \frac{1}{<\tau_i>_{HC}} + \frac{1}{<\tau_i>_{PD}} + \frac{1}{<\tau_i>_{CX}} \quad . \tag{4.7}$$

We assume that the thermal conduction is neoclassical [10,11], and estimate the energy loss time as $<\tau_i>_{HC} \simeq a^2/(10K_{\perp i})$. The loss times $<\tau_i>_{PD}$ and $<\tau_i>_{CX}$ are approximately estimated as $<\tau_i>_{PD} = 1/(n_{no}<\sigma_{ion}v_e>)$ and $<\tau_i>_{CX} = 1/(n_{no}<\sigma_{CX}v_i>)$, where σ_{ion} and σ_{CX} are the cross sections of ionization and charge exchange, respectively. In the experiments, the neutral atom density n_{no} on the plasma axis is not obtained experimentally. We evaluate it by $n_{no} = 1.8 \times 10^{28}/[n_{eo}(cm^{-3})]^{1.44}$ in cm^{-3} [12]. The relation between T_{i0}/T_{e0} and $<\tau_{eq}>/<\tau_i>_{th}$ is shown in Fig.8, where

$\langle\tau_i\rangle_{th}$ is the ion energy confinement time calculated by Eq.(4.7). The temperature ratio T_{i0}/T_{e0} agrees with Eq.(4.6) very well.

4.5 Gross Energy Confinement Time

The gross energy confinement time is evaluated as follows,

$$\langle\tau_E\rangle = \frac{W}{P_{OH} - dW/dt} \quad . \tag{4.8}$$

Here P_{OH} and W are the ohmic input power and total thermal energy, and given as

$$W = W_e + W_i \quad ,$$

$$P_{OH} = V_{loop}\, I_p - d(L_p I_p^2/2)/dt \quad , \tag{4.9}$$

where V_{loop} is loop voltage, L_p is plasma inductance and I_p is plasma current. The relation between $\langle\tau_E\rangle/\bar{n}_e$ and q(a) is shown in Fig.9. Figure 9 shows approximately $\langle\tau_E\rangle/\bar{n}_e \propto q(a)^{1/2}$. From this figure, the scaling law of $\langle\tau_E\rangle$ similar to those in ORMAK [13] and ALCATOR [14] is derived and $\langle\tau_E\rangle$ reaches about 14 msec (Fig.10).

5. TEMPORAL EVOLUTION OF TYPICAL PLASMA PARAMETERS IN DISCHARGES WITH MUCH GAS INJECTION

In much gas injection two types of discharges appear on the same discharge conditions except for the slight difference of feedback control condition of plasma position, where the initial filling pressure is 2.0×10^{-4} Torr H_2 and the influx by the gas injection corresponds to the pressure of about 1.5×10^{-3} TorrH_2 at 40 msec. One is the well-centered and high density discharge where no MHD oscillation appears in

the quasi-steady state (case A). In the other type of discharge (case B), the plasma position is shifted outwardly by about 5 mm in comparison with case A, where the m = 2 MHD oscillation exists continuously.

Figure 11 shows the time variations of plasma current and loop voltage, perturbations of poloidal field, central electron and ion temperatures, central electron density, and the profile shape factor of electron density ($S_n = n_{e0}/\bar{n}_e = 1/\int_0^1 (n_e(x)/n_{e0})dx$). The electron and ion temperatures have not the remarkable difference in both cases. However, the electron density of case B is limited at about half of case A because of the m = 2 MHD oscillations. The quantity S_n is evaluated as $S_n = I_L/m_o$, where I_L is the integrated value of scattered light sepctrum and m_o is the number of fringe obtained from the microwave interferometer. It is noted that the 4 mm microwave is cut off in the plasma which has the density greater than 6.89×10^{13} cm^{-3} (n_{ec}). In the experiments, data of microwave interferometer (m_o) are compared with data of Thomson scattering corresponding to the central electron density (I_L) in the range of $n_e < n_{ec}$. When the microwave is cut off, I_L and the profile of I_L are measured by Thomson scattering and the electron density is estimated by using the value of S_n in $n_e < n_{ec}$. The scale of S_n is adjusted so that S_n should be equal to 1.5 for the parabolic profile. As seen from the time variation the density profile is nearly parabolic during the discharge in case B, but the profile of case A changes remarkably. The remarkably broad profile is predicted at the current rising phase (t = 20~50 msec). On the other hand the results of Thomson scattering suggest that the electron density has a weak hollow profile at that phase (Fig.12).

In Fig.13, we show the time evolutions of $\langle\tau_E\rangle$, β_p and $\langle Z_{eff}\rangle$ comparing cases A and B, where we assume $T_e = T_{e0}(1 - x^2)^2$, $T_i = T_{i0}(1 - x^2)^2$

and $n_e = n_{e0}(1 - x^2)$ for case A, and $T_e = T_{e0}(1 - x^2)^3$, $T_i = T_{i0}(1 - x^2)^3$ and $n_e = n_{e0}(1 - x^2)$ for case B. The gross energy confinement times of both cases are also plotted on the empirical scaling law shown in Fig.10. It should be noted that $\langle Z_{eff} \rangle$ included the error of about 40 % from uncertainty of the temperature profiles. Therefore, it seems that the values of $\langle Z_{eff} \rangle$ in both cases have not the obvious difference.

6. DISRUPTIVE INSTABILITY IN HIGH DENSITY DISCHARGE

The electron density can be raised by using the pulsed gas injection method. The intense injection of cold neutral gas which aims the high density plasma tends to cause disruptive instaiblity because of shrinkage by radiative cooling of plasma periphery. The electron density of tokamak plasma is limited by the disruptive instaiblity. In this section we demonstrate the suppression of the disruptive instaiblity caused by the intense injection of cold gas.

Figure 14 shows the disruptive discharge triggered by the additional gas injection from 75 msec (case I). The gas influx by the injection corresponds to the pressure of about 3.0×10^{-3} TorrH_2 at 105 msec. The plasma shrinkage by the gas injection is clearly observed by the TV camera with the filter which passes the light around H_α line. The image obtained at the time marked by an arrow in Fig.14(a) is also shown in Fig.14(b). The effective plasma radius corresponding to the hot region contracts to about one third of limiter radius. The electron density cannot be obtained more than 40 fringes due to cut off of microwave that results from the remarkable shrinkage of plasma (shown in Fig.18 later). The time of cut off of microwave agrees with the peak of central electron density obtained from Thomson scattering. We can evaluate the maximum

density by the cut off point related to the disruptive instability. The intense cooling of plasma periphery can be avoided by the additional heating concentrated in the plasma peripheral region. We adopt a rapid increase of the plasma current in the course of discharge as the above-mentioned additional heating method.

We examine by the observation of MHD oscillations whether the remarkable broadening or considerable skin effect of current density profile is caused by the second rapid rise of plasma current. Two different discharge characteristics are shown in Fig.15. When the plasma current is increased rapidly in the course of discahrge without intense gas injection, the m = 6, 5 4 and 3 MHD oscillations which coincide with the safety factor at the plasma surface q(a) are successively observed at the second rising phase of plasma current (case IIA). The mode number is considerably smaller than q(a) at about 15 msec from the start of second current rise. It means that the broad or skin profile of plasma current density has been effectively changed to the peaky profile at the time. On the other hand, the above oscillations do not appear in the discharge which has not the second current rise but the current corresponding to appearance of m = 4 oscillation in case II A (case IIB). It is concluded that the oscillations have been excited by the broadening or skin effect of current density profile.

The appropriate combination between the shrinking effect by the gas injection and the effective heating of peripheral region by the rapid rise of current will suppress the disruptive instabilities. Figure 16 shows the discharge where both the intense gas injection and the second rapid rise of current are applied (case IIIA). Though the safety factor q(a) decreases to 2.2, the MHD oscillation is not any excited and the disruptive instability is completely suppressed. The image of H_α light

by the TV camera shows that the second current rise prevents the hot plasma region from shrinking.

Moreover, we examine the required increment of the second current rise to suppress the disruptive instaiblities completely. The delay time (τ_{DIS}) of appearance of disruptive instabilities by the second current rise are shown in Fig.17 as a function of the increment of the second rise (ΔI_p). When ΔI_p increases, τ_{DIS} also increases linearly. However, if ΔI_p is greater than a certain threshold $(\Delta I_p)_c$, the disruptive instabilities are suppressed completely. On the other hand, the upper limit of ΔI_p will be determined by reduction of safety factor q(a). In case IIIA, the increment of the second current rise is ΔI_p = 77 kA, and q(a) decreases to 2.2 without any MHD oscillations and disruptive instabilities, even though the line-averaged electron density attains to 6 x 10^{13} cm^{-3} as described later. This fact suggests that the considerably broad profile of current density and high electron density discharges can be realized by the above procedure.

In Fig.18 we show the time variations of central electron temperature, intensity of OIV line (3737 Å), the profile parameter of electron density S_n defined in section 5 and electron density as the number of fringes comparing the discharges of cases I, IIA, IIIA and IIIB with one another. The electron density is limited at about 40 fringes owing to the remarkable peaking of density profile for both discharges of the low current (case I) and the one of high current (case IIIB) without the second current rise. By the application of the second current rise (case IIIA) the number of fringes reaches about 68 ($\bar{n}_e \simeq 6 \times 10^{13}$ cm^{-3}) without the remarkable desorption of oxygen. In this case the electron density profile is also considered to be very broad.

From the above results, it is expected that the appropriate combina-

tion of the pulsed gas injection with effective heating method of plasma peripheral region will raise up the density limit of tokamak plasma determined by the disruptive instability.

7. SUMMARY

The results obtained in the present experiment are summarized as follows:

(1) The line-averaged density $\bar{n}_e$ is changed from 1 x 10^{13} cm^{-3} to 5 x 10^{13} cm^{-3}. The energy confinement time $<\tau_E>$ increases in proportion to $\bar{n}_e q(a)^{1/2}$ in the range of $q(a) = 2.2 \sim 4.6$ and has reached 14 msec.

(2) The central electron temperature T_{e0} increases as plasma current increases in the low density regime ($\bar{n}_e \lesssim 2.5 \times 10^{13}$ cm^{-3}). When the electron density increases, T_{e0} depends on not only I_p but also q(a).

(3) The ion temperature agrees well with the Artsimovich's scaling law.

(4) The averaged ionic charge derived from plasma conductivity is 1 to 2 in the regime of small streaming parameter ($<v_d/v_{the}> = 0.01$-0.08).

(5) The ratio of ion temperature to electron temperature T_{i0}/T_{e0} is considerably large and $T_{i0}/T_{e0} \gtrsim 0.5$ for all discharges. This result means that the ion energy confinement time $<\tau_i>$ is greater than the electron-ion energy relaxation time $<\tau_{eq}>$.

(6) The m = 2 MHD mode deteriorates the plasma confinement. In such discharge, the electron and ion temperatures do not decrease considerably, but the electron density is limited at half of density in stable high density discharge due to enhancement of particle diffusion.

(7) The disruptive instabilities due to the intense gas injection are suppressed completely by the second rapid rise of plasma current.

The appropriate combination of the pulsed gas injection with the effective heating method of the peripheral region of plasma raises the electron density limit of tokamak palsma due tothe disruptive instability.

REFERENCES

[1] JIPP T-II group, in Plasma Phys. and Contr. Nucl. Fus. Res. (Proc. 6th Int. Conf. Berchtesgaden, 1976) Paper D3.

[2] V. S. Mukhovatov and V. D. Shafranov, Nucl. Fusion 11 (1971) 605.

[3] S. Itoh, K. Toi and K. Matsuura, to be published in Japan. J. Appl. Phys.

[4] N. D. Vinogradova et al., in Plasma Phys. and Contr. Nucl. Fus. Res. (Proc. 4th Int. Conf. Madison, 1971) Paper F8.

[5] L. A. Berry et al., in Plasma Phys. and Contr. Nucl. Fus. Res. (Proc. 5th Int. Conf. Tokyo, 1971) Paper A5-2.

[6] J. W. M. Paul et al., in Plasma Phys. and Contr. Nucl. Fus. Res. (Proc. 6th Int. Conf. Berchtesgaden, 1976) Paper A17.

[7] M. P. Petrov, Sov. Phys. Tech. Phys. 13 (1966) 708.

[8] G. J. Boxman et al., in Contr. Fus. and Plasma Phys. (Proc. 7th Europ. Conf. Lausanne, 1975) II, 14

[9] B. Coppi et al., Nucl. Fusion 16 (1976) 309.

[10] F. L. Hinton and M. N. Rosenbluth, Phys. Fluids 16 (1973) 836.

[11] R. D. Hazeltine and F. L. Hinton, Phys. Fluids 16 (1973) 1883.

[12] P. E. Stott, Plasma Phys. 18 (1976) 251.

[13] L. A. Berry et al., in Plasma Phys. and Contr. Nucl. Fus. Res. (Proc. 6th Int. Conf. Berchtesgaden, 1976) Paper A4-1.

[14] E. Apgar et al., ibid., Paper A5.

TABLE AND FIGURE CAPTIONS

Table 1. The basic parameters of the JIPP T-II device.

Fig.1. Cross sectional view of the JIPP T-II device.

Fig.2. Schematic view of vacuum system, gas filling system and diagnostic instruments used in the present experiment.

Fig.3. Typical discharge with pulsed gas injection. V_{piezo} is the voltage applied to piezo-electric crystal. B_t = 30 kG, P_{fl} = 2.8×10^{-4} TorrH_2.

Fig.4. Dependence of central electron temperature on plasma current for various ranges of electron density. B_t=15∿30 kG.

Fig.5. Dependence of central electron temperature divided by plasma current on the safety factor at the plasma surface. This figure is obtained from Fig.4.

Fig.6. Comparison of central ion temperatures with Artsimovich's scaling law. B_t = 15∿30 kG, I_p = 60∿160 kA.

Fig.7. Dependence of the ratio of Spitzer's conductivity to experimental conductivity on averaged streaming parameter. v_d and v_{the} are the drift velocity and electron thermal velocity, respectively. < > denotes the average over the plasma cross section. The spread of data means the uncertainty of electron temperature and density profiles, and for the comparatively low density operation ($\langle v_d/v_{the} \rangle > 0.02$), $T_e = T_{e0}(1 - x^2)^n$, $1 \leqq n \leqq 2$, $n_e = n_{e0}(1 - x^2)$ and for high density operation ($\langle v_d/v_{the} \rangle < 0.02$), $T_e = T_{e0}(1 - x^2)^n$, $2 \leqq n \leqq 3$, $n_e = n_{e0}(1 - x^2)$ and current density profile $j \propto T_e^{3/2}$. B_t = 15∿30 kG, I_p = 60∿160 kA.

Fig.8. Dependence of the temperature ratio T_{i0}/T_{e0} on the ratio of electron-ion energy relaxation time to ion energy confinement time $\langle\tau_{eq}\rangle/\langle\tau_i\rangle_{th}$, where $\langle\tau_i\rangle_{th}$ is estimated theoretically. The curve shows the relation of $T_{i0}/T_{e0} = 1/(1 + \langle\tau_{eq}\rangle/\langle\tau_i\rangle_{th})$. B_t= 15~30 kG, I_p = 60~160 kA.

Fig.9. Dependence of ratio of gross energy confinement time to line-averaged electron density on the safety factor. B_t = 15~30 kG, I_p = 60~160 kA.

Fig.10. Empirical scaling of gross energy confinement time derived from Fig.9. The solid lines 1 and 2 show the scaling laws in ALCATOR and ORMAK, respectively.

Fig.11. Comparison between the stable discharge (case A) and discharge which m = 2 mode appears (case B) in the much gas injection experiment. B_t = 30 kG, $P_{fl} = 2.0 \times 10^{-4}$ TorrH_2.

Fig.12. Radial profiles of electron temperature and density obtained by Thomson scattering for cases A and B.

Fig.13. Temporal evolutions of $\langle\tau_E\rangle$, β_p and $\langle Z_{eff}\rangle$ for cases A and B.

Fig.14. The disruptive discharge (case I) excited by the intense gas injection. The photograph (b) is the H_α image monitored at the time shown by an arrow in (a), using the TV camera. B_t = 30 kG, $P_{fl} = 1.6 \times 10^{-4}$ TorrH_2.

Fig.15. The discharge with the second current rise without intense gas injection (case IIA). In case IIA, a remarkable broadening or skin effect of current density profile appears. The discharge which has not the second current rise but the current corresponding to appearance of m = 4 mode is also shown (case IIB). B_t = 30 kG, $P_{fl} = 1.6 \times 10^{-4}$ TorrH_2.

Fig.16. The discharge with both intense gas injection and the second rapid rise of current (case IIIA). The photograph is the H_α image monitored at the time shown by an arrow. The discharge which has current approximately corresponding to the value of discharge with the second current rise is also shown (case IIIB). B_t = 30 kG, P_{fl} = 1.6 x 10^{-4} TorrH_2.

Fig.17. Relation between delay time of appearance of disruptive instability by second current rise and the increment of second current rise.

Fig.18. Time variations of central electron temperature, intensity of OIV line (3737 Å) and the profile shape parameter S_n defined in section 5 for the cases I and IIIA, and electron density as the number of fringes for cases I, IIA, IIIA and IIIB.

Table 1.

Major Radius:	R_o = 91 cm
Limiter Radius:	a_L = 7~17 cm (variable)
Minor Radius of Vacuum Chamber:	20 cm
Toroidal Field:	B_t = 30 kG
Maximum Ripple of B_t over the Plasma Cross Section:	$\delta B_t/B_t$ = 0.5%
Helical Field (ℓ=2, m=4 winding):	$\iota/2\pi$ = 0.3 for B_t = 20 kG
	$\iota/2\pi$ = 0.1 for B_t = 30 kG
Stational Vertical Field:	B_{vd} = 1100 G
Negative Pulsed Vertical Field:	B_{vp} = -1100 G
Feedback-Controlled Vertical Field:	B_{vf} = -10 ∿ -210 G
Time Constant of Resistive Shell for Vertical Field:	τ_s = 5.2 msec
Feedback-Controlled Horizontal Field:	B_H = 60 G
Capacitor Power Supply for Primary Windings:	Stored Energy of 1st Bank = 100 kJ
	Stored Energy of 2nd Bank = 160 kJ
	Stored Energy of 3rd Bank = 100 kJ
Flux of Current Transformer without Premagnetization:	0.58 Volt·sec
Baking Temperature of Pumping System and Gas Filling System:	250°C ∿ 300°C
Baking Temperature of Vacuum Chamber and Extension Ports:	350°C

Molybdenum limiter is processed by electron beam and outgassed in vacuum oven.

Total Pumping Speed at the Evacuation Port (Turbo-Molecular Pump, Sputter Ion Pump, Titanium Getter Pump):	500 ℓ/sec
Base Pressure:	1.2×10^{-9} Torr

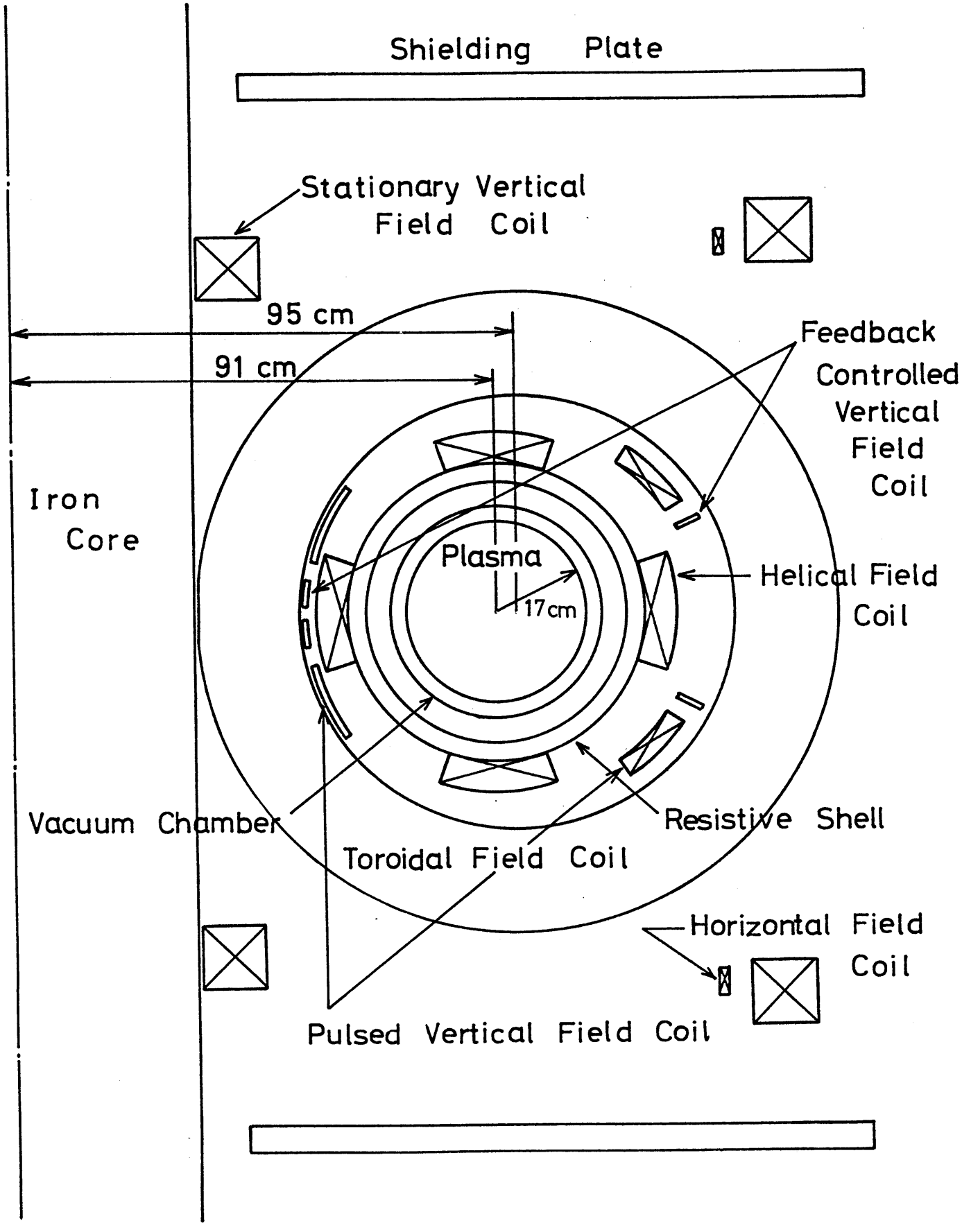
Shielding Plate
Stationary Vertical Field Coil
95 cm
91 cm
Feedback Controlled Vertical Field Coil
Iron Core
Plasma
17cm
Helical Field Coil
Vacuum Chamber
Resistive Shell
Toroidal Field Coil
Horizontal Field Coil
Pulsed Vertical Field Coil

Fig. 1

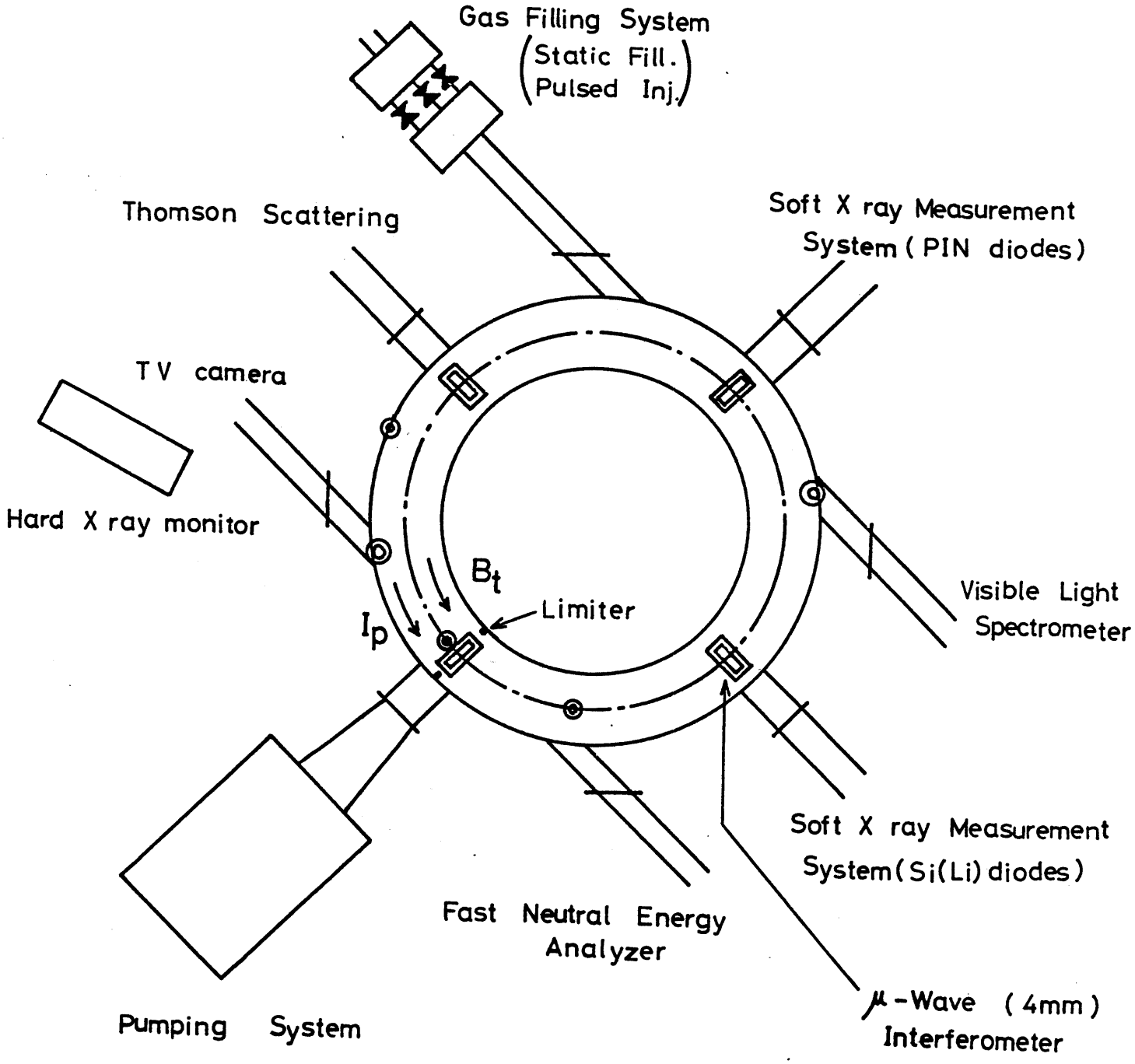
Gas Filling System
(Static Fill.
Pulsed Inj.)
Thomson Scattering
Soft X ray Measurement
System (PIN diodes)
TV camera
Hard X ray monitor
B_t
I_p
Limiter
Visible Light
Spectrometer
Soft X ray Measurement
System(Si(Li) diodes)
Fast Neutral Energy
Analyzer
μ-Wave (4mm)
Interferometer
Pumping System

Fig. 2

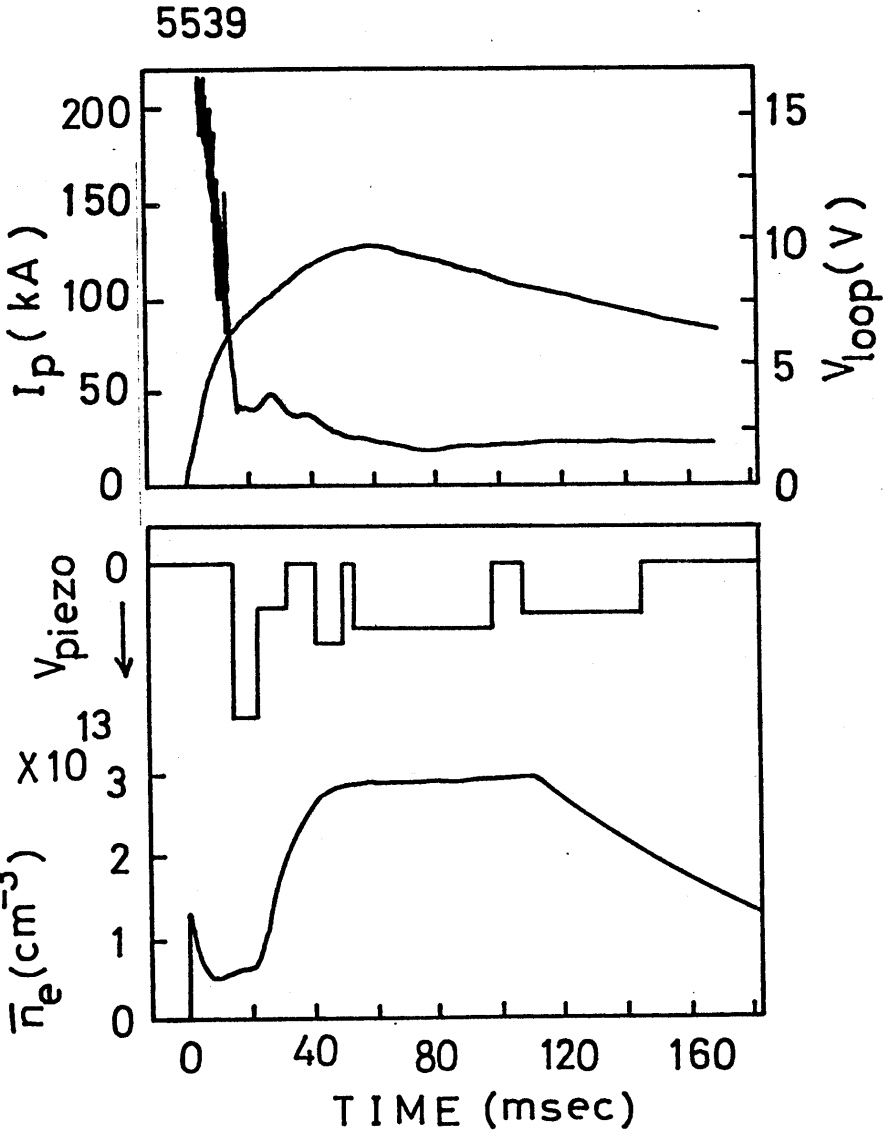
5539
200
150
100
50
0
I_p (kA)
15
10
5
0
V_{loop} (V)
V_{piezo}
0
X10 13
3
2
1
0
$\bar{n}_e(cm^{-3})$
0
40
80
120
160
TIME (msec)

Fig. 3

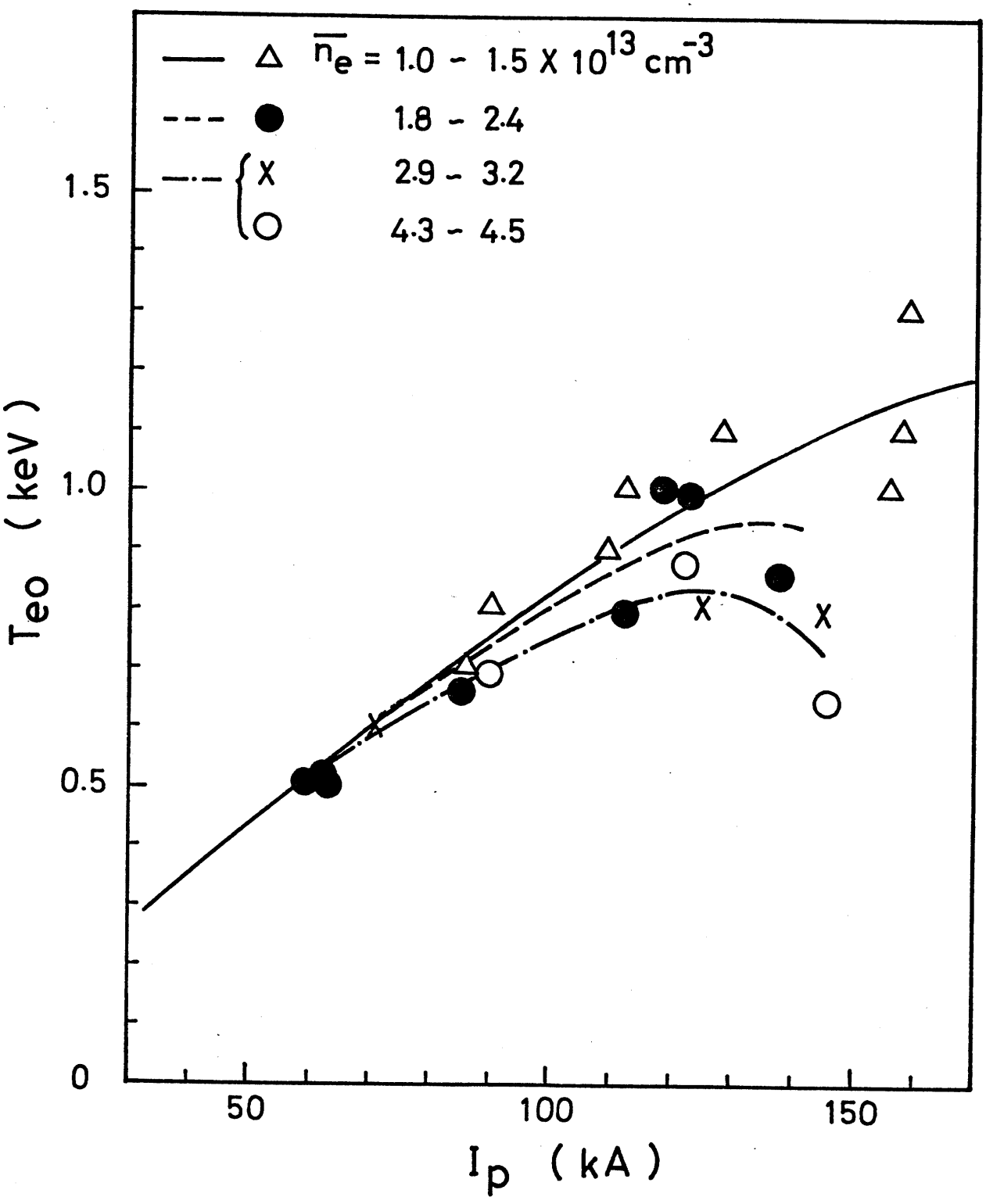
$\bar{n}_e$ = 1.0 - 1.5 X 10^{13} cm^{-3}
1.8 - 2.4
2.9 - 3.2
4.3 - 4.5
1.5
1.0
0.5
0
T_{eo} (keV)
50
100
150
I_p (kA)

Fig. 4

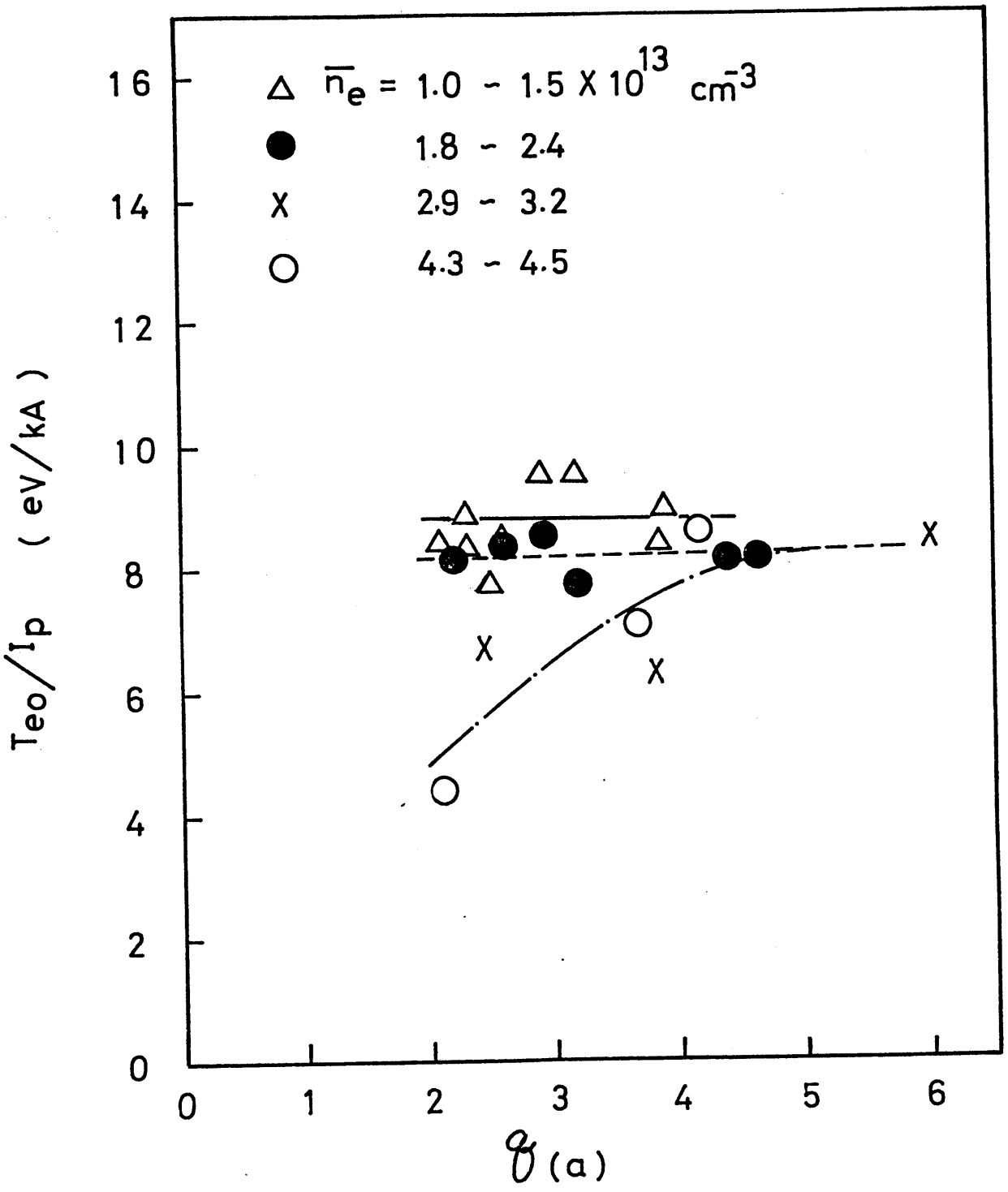
$\bar{n}_e$ = 1.0 ~ 1.5 X 10^{13} cm^{-3}
1.8 ~ 2.4
2.9 ~ 3.2
4.3 ~ 4.5
T_{eo}/I_p (eV/kA)
ρ (a)
0
2
4
6
8
10
12
14
16
0
1
2
3
4
5
6

Fig. 5

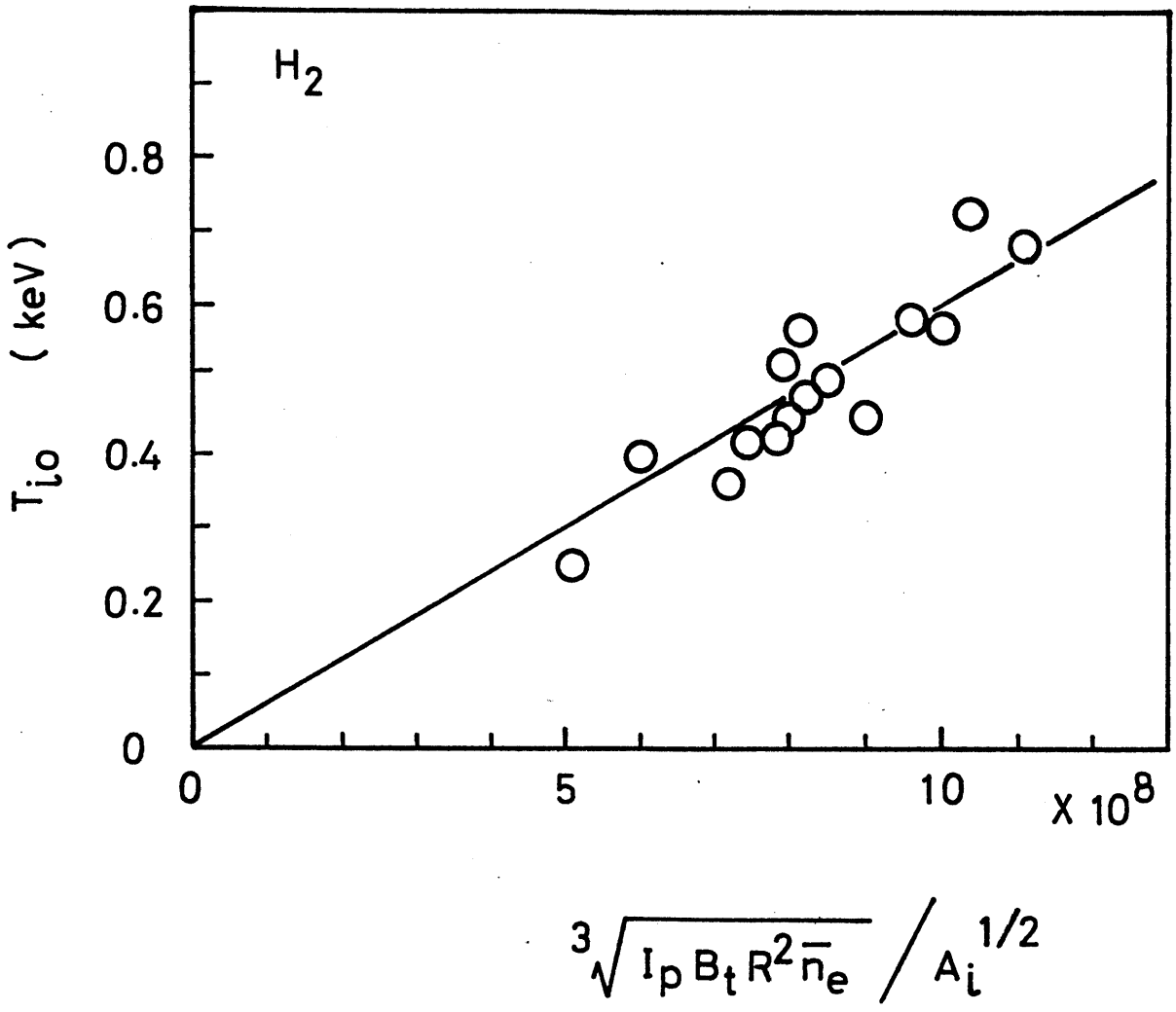

Fig. 6

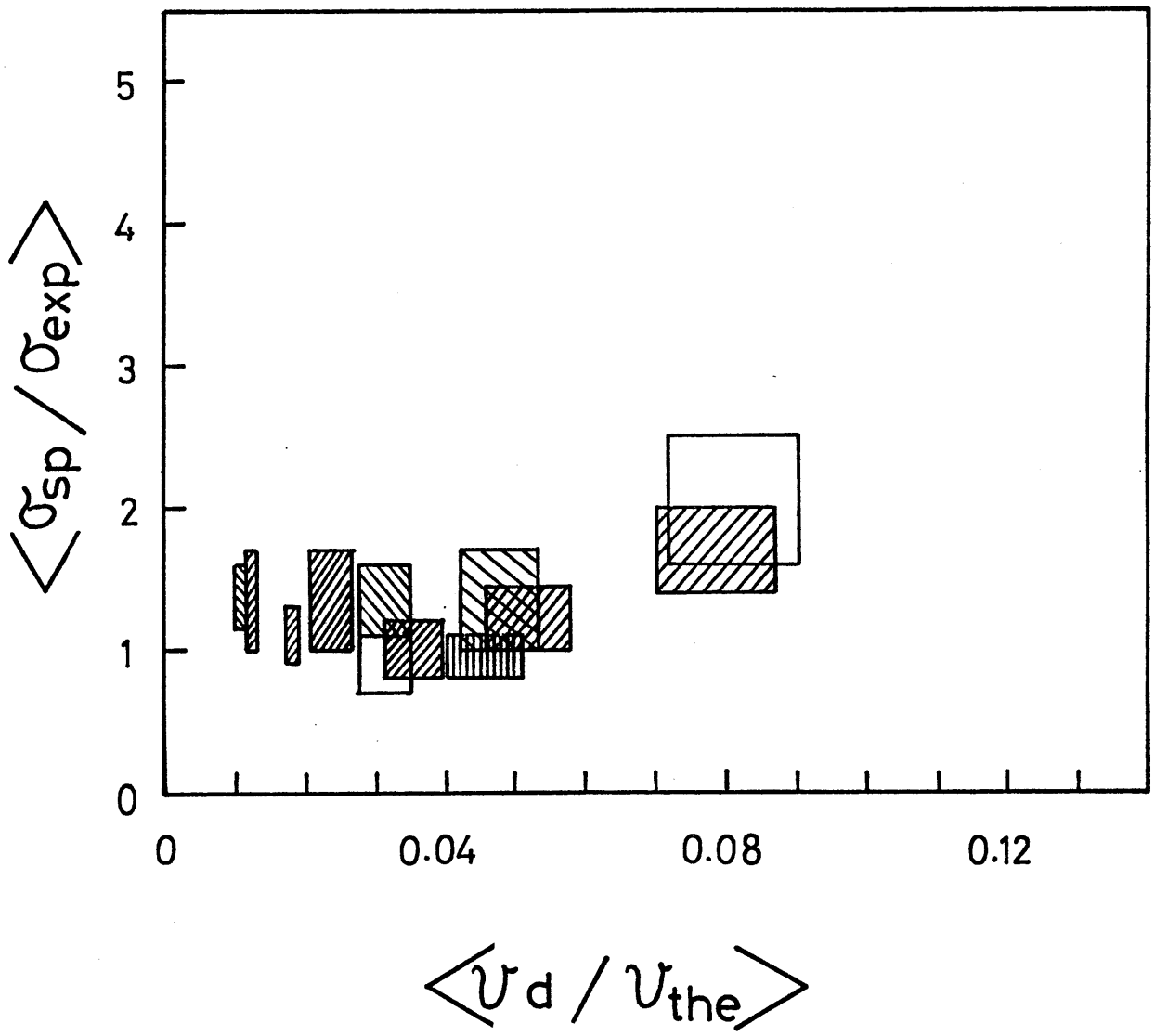

Fig.7

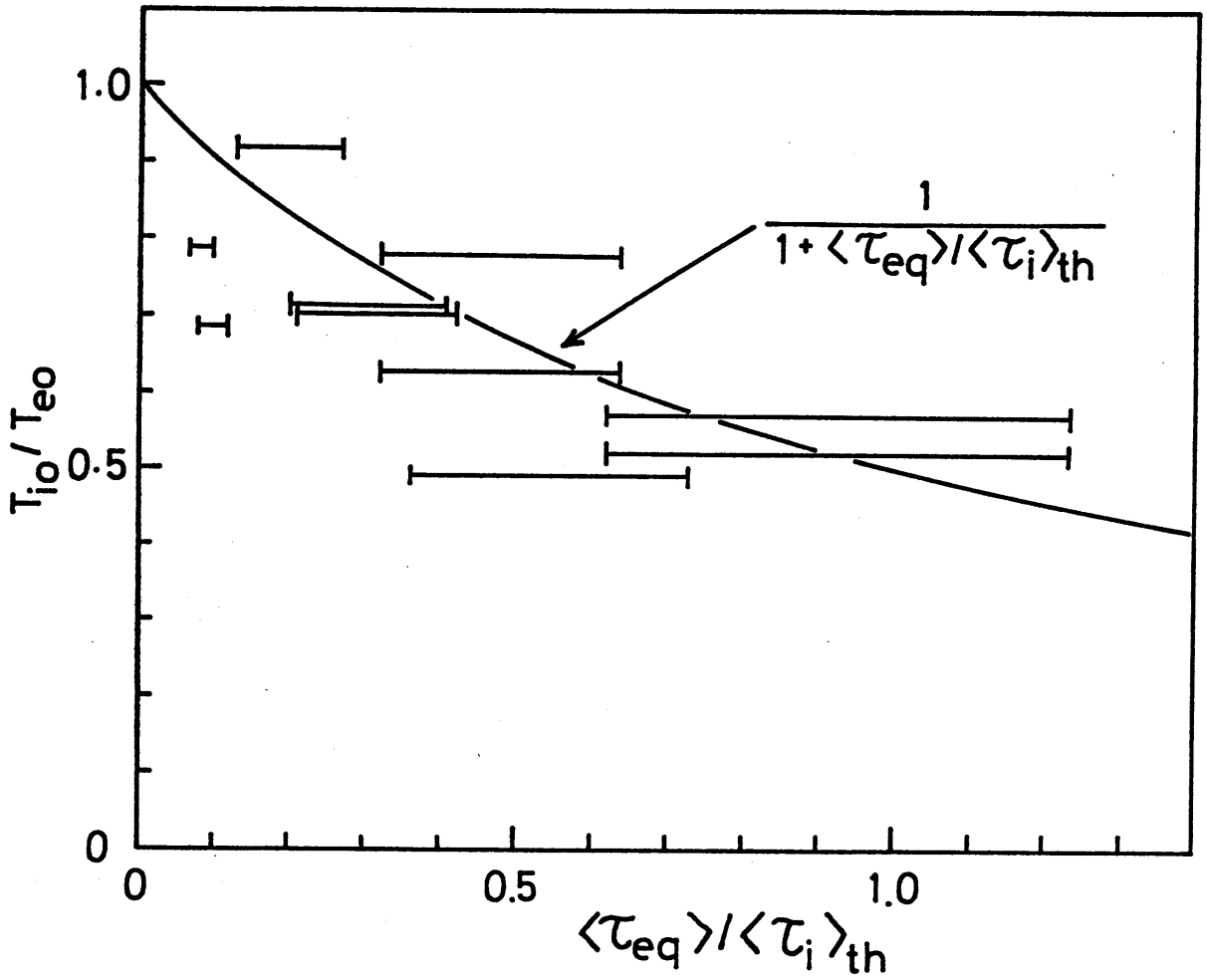
1.0
0.5
0
T_{io}/T_{eo}
$\frac{1}{1+\langle\tau_{eq}\rangle/\langle\tau_i\rangle_{th}}$
0
0.5
1.0
$\langle\tau_{eq}\rangle/\langle\tau_i\rangle_{th}$

Fig.8

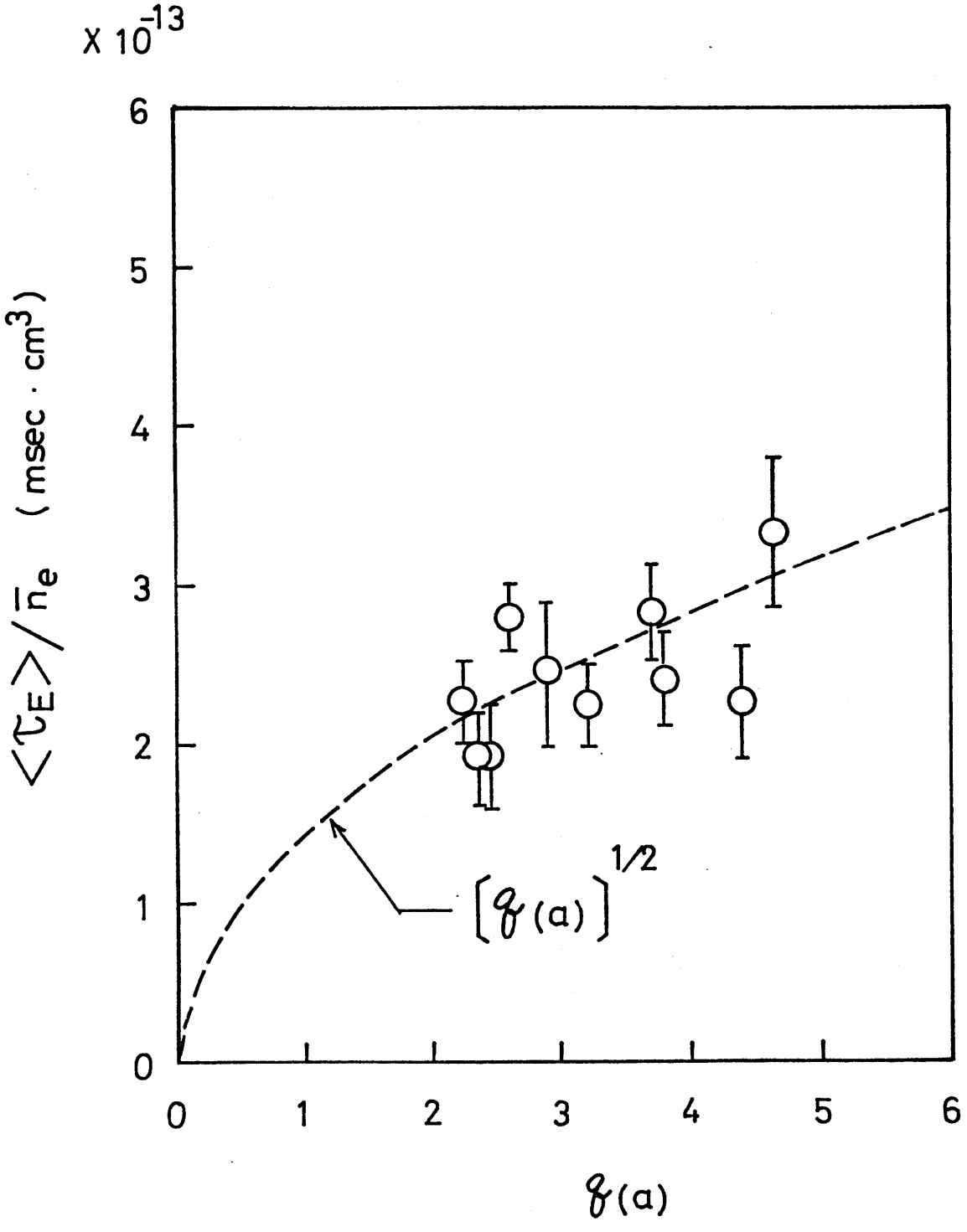

Fig.9

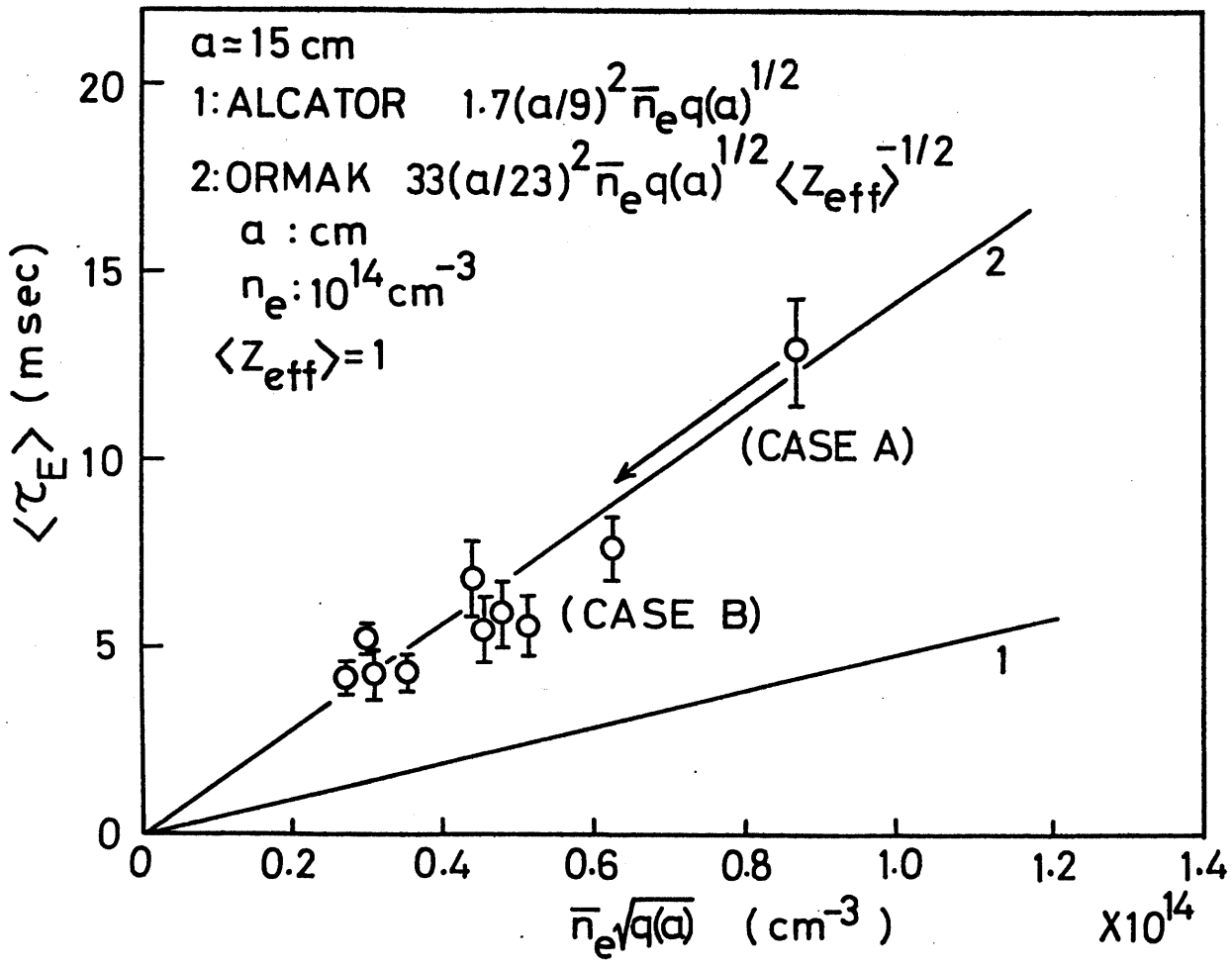
a≈15 cm
1: ALCATOR 1·7(a/9)^2 $\bar{n}_e q(a)^{1/2}$
2: ORMAK 33(a/23)^2 $\bar{n}_e q(a)^{1/2} \langle Z_{eff}\rangle^{-1/2}$
a : cm
n_e: 10^{14} cm^{-3}
$\langle Z_{eff}\rangle$=1
$\langle \tau_E \rangle$ (msec)
(CASE A)
(CASE B)
1
2
0
5
10
15
20
0
0.2
0.4
0.6
0.8
1.0
1.2
1.4
$\bar{n}_e\sqrt{q(a)}$ (cm^{-3}) X10^{14}

Fig.10

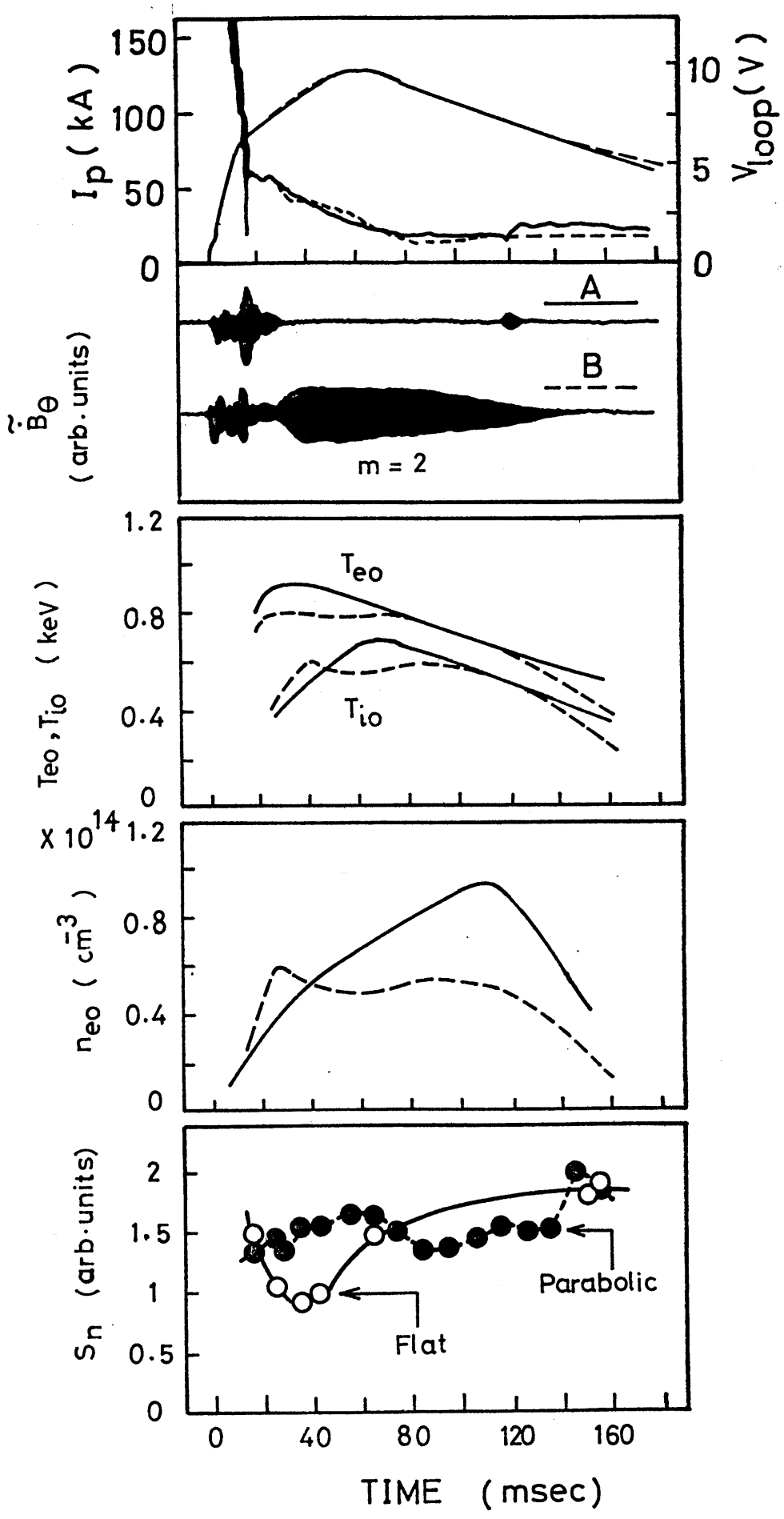
150
100
50
0
I_p (kA)
10
5
0
V_{loop} (V)
A
B
m = 2
$\tilde{B}_\theta$ (arb. units)
1.2
0.8
0.4
0
T_{eo}
T_{io}
T_{eo}, T_{io} (keV)
x 10^{14}
1.2
0.8
0.4
0
n_{eo} (cm^{-3})
2
1.5
1
0.5
0
S_n (arb·units)
Parabolic
Flat
0
40
80
120
160
TIME (msec)

Fig.11

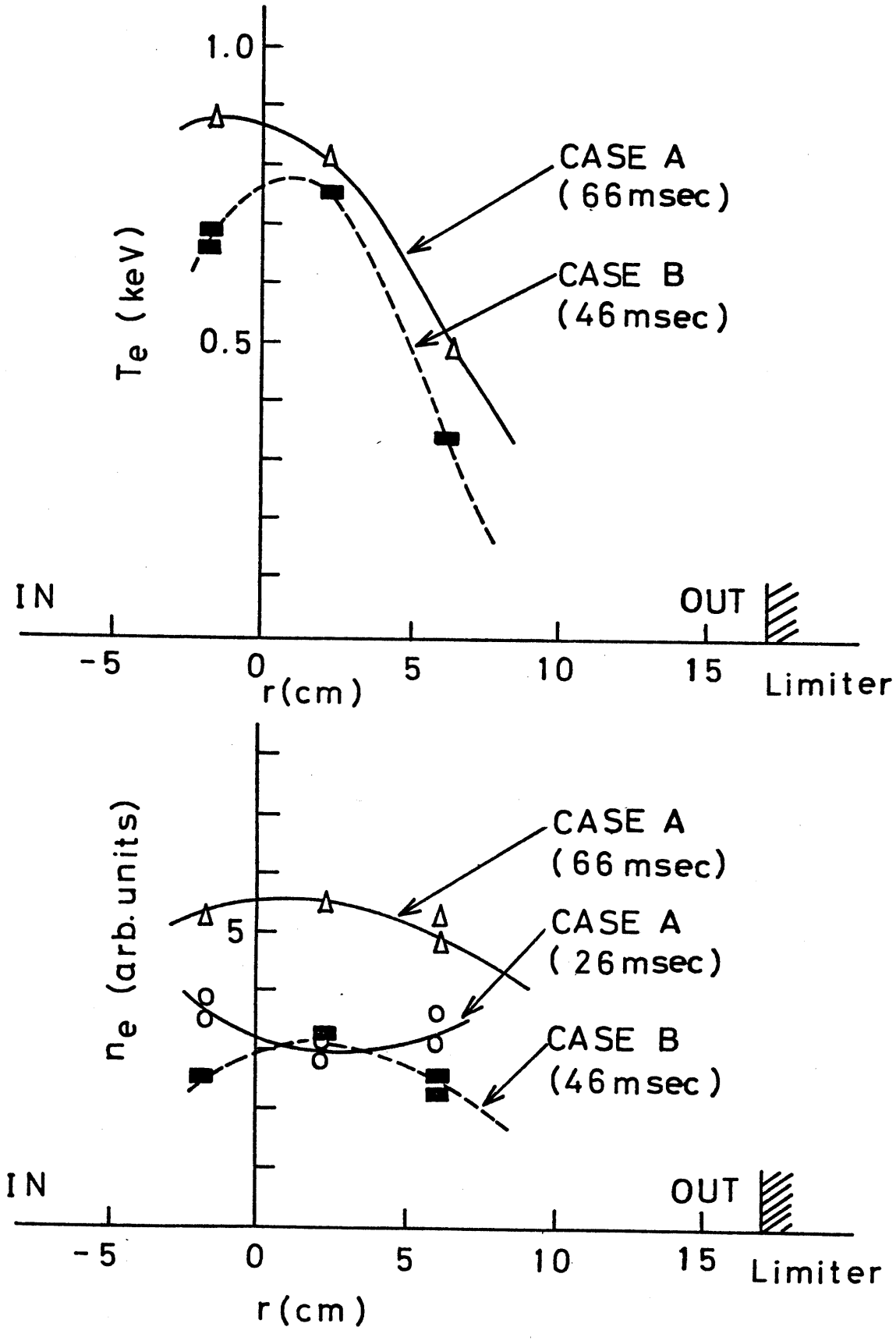
1.0
0.5
T_e (keV)
CASE A
(66msec)
CASE B
(46msec)
IN
OUT
-5
0
5
10
15
r(cm)
Limiter
n_e (arb.units)
5
CASE A
(66 msec)
CASE A
(26msec)
CASE B
(46msec)
IN
OUT
-5
0
5
10
15
Limiter
r(cm)

Fig.12

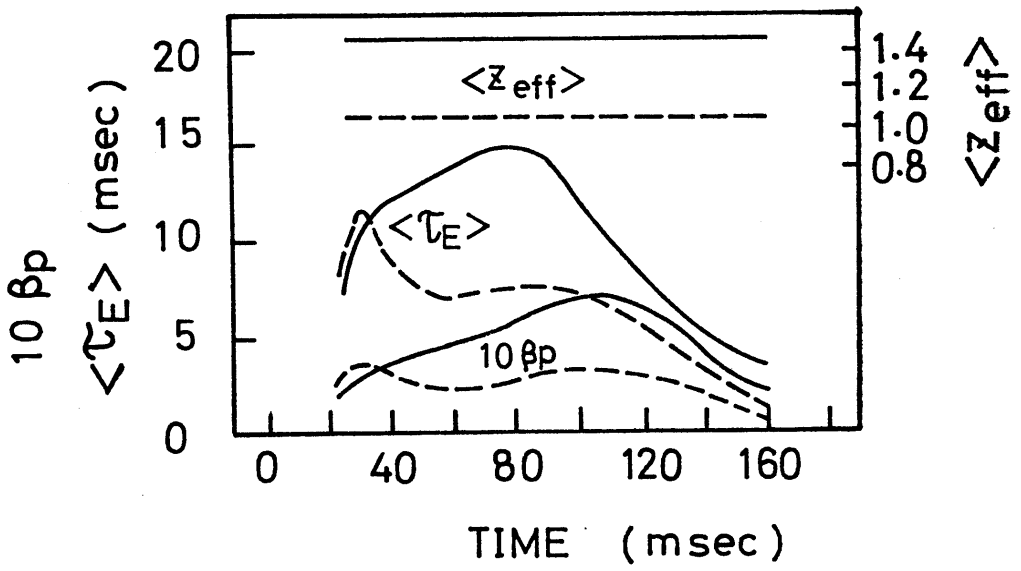
20
15
10
5
0
10 βp
<τE> (msec)
<Zeff>
<τE>
10 βp
1.4
1.2
1.0
0.8
<Zeff>
0
40
80
120
160
TIME (msec)

Fig.13

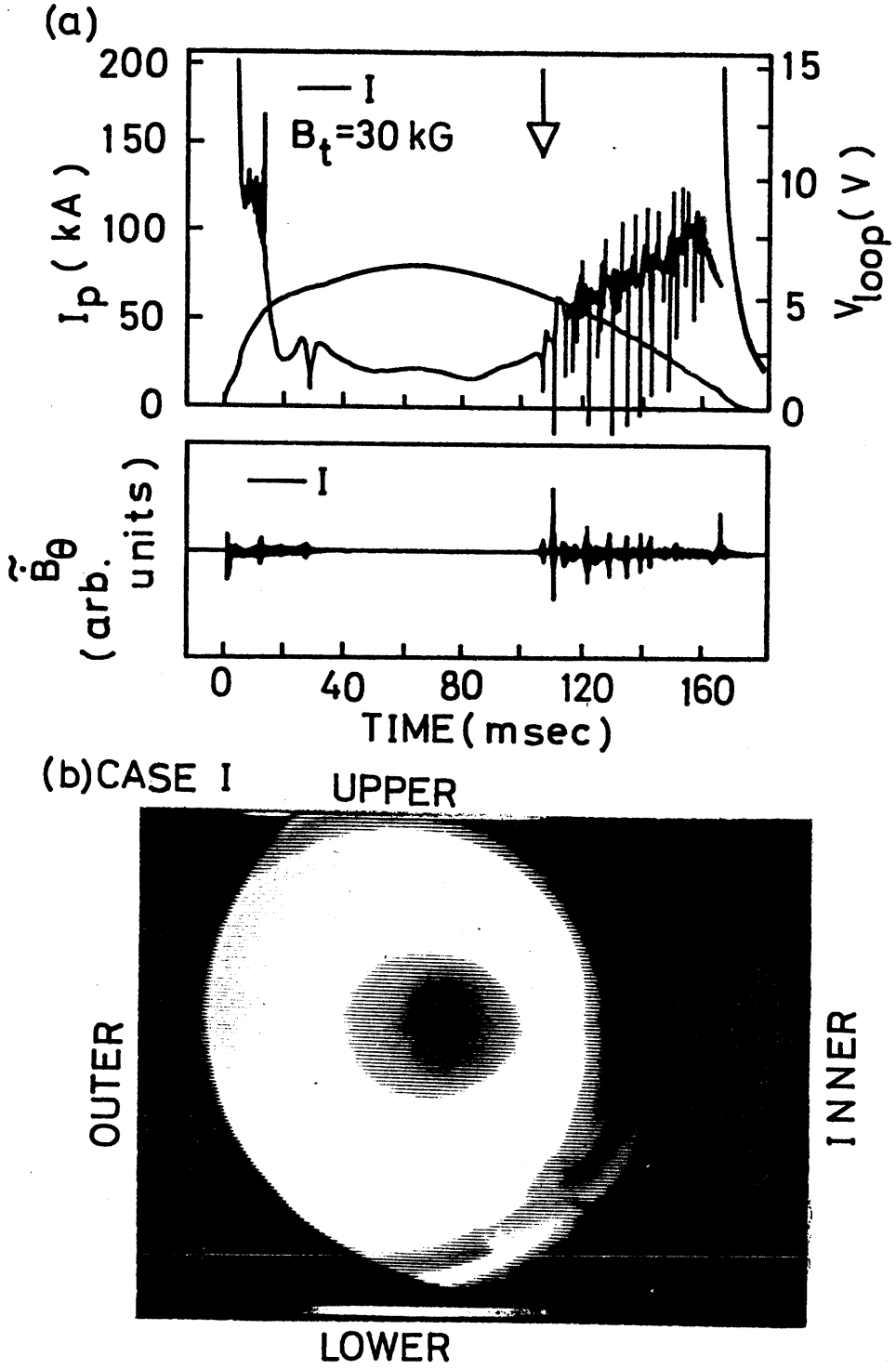
(a)
200
150
100
50
0
I_p (kA)
— I
B_t=30 kG
15
10
5
0
V_{loop} (V)
— I
$\tilde{B}_\theta$ (arb. units)
0
40
80
120
160
TIME (msec)
(b)CASE I
UPPER
OUTER
INNER
LOWER

Fig.14

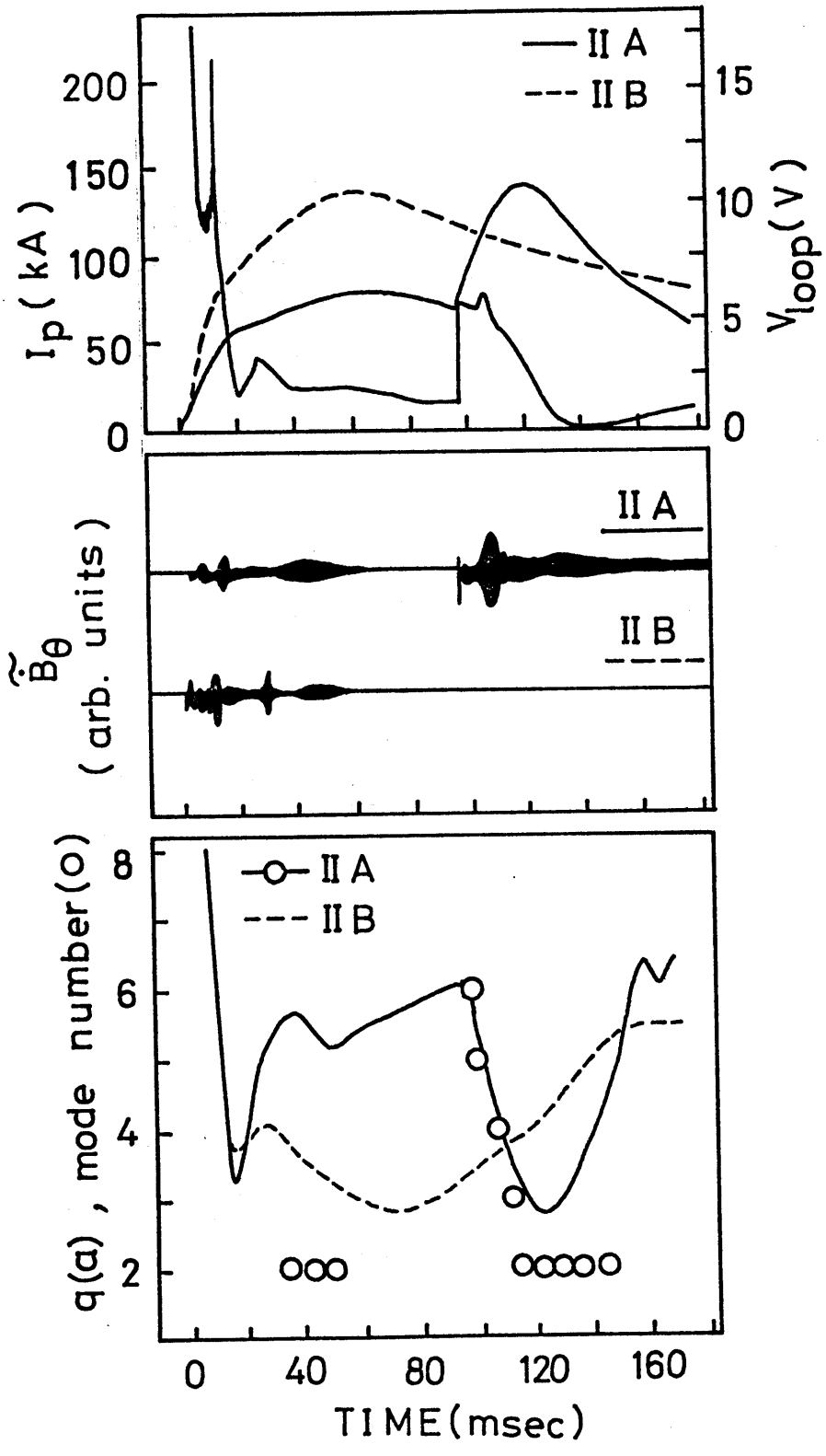
II A
II B
200
150
100
50
0
I_p (kA)
15
10
5
0
V_{loop} (V)
II A
II B
$\tilde{B}_\theta$ (arb. units)
II A
II B
8
6
4
2
q(a) , mode number(o)
0
40
80
120
160
TIME(msec)

Fig.15

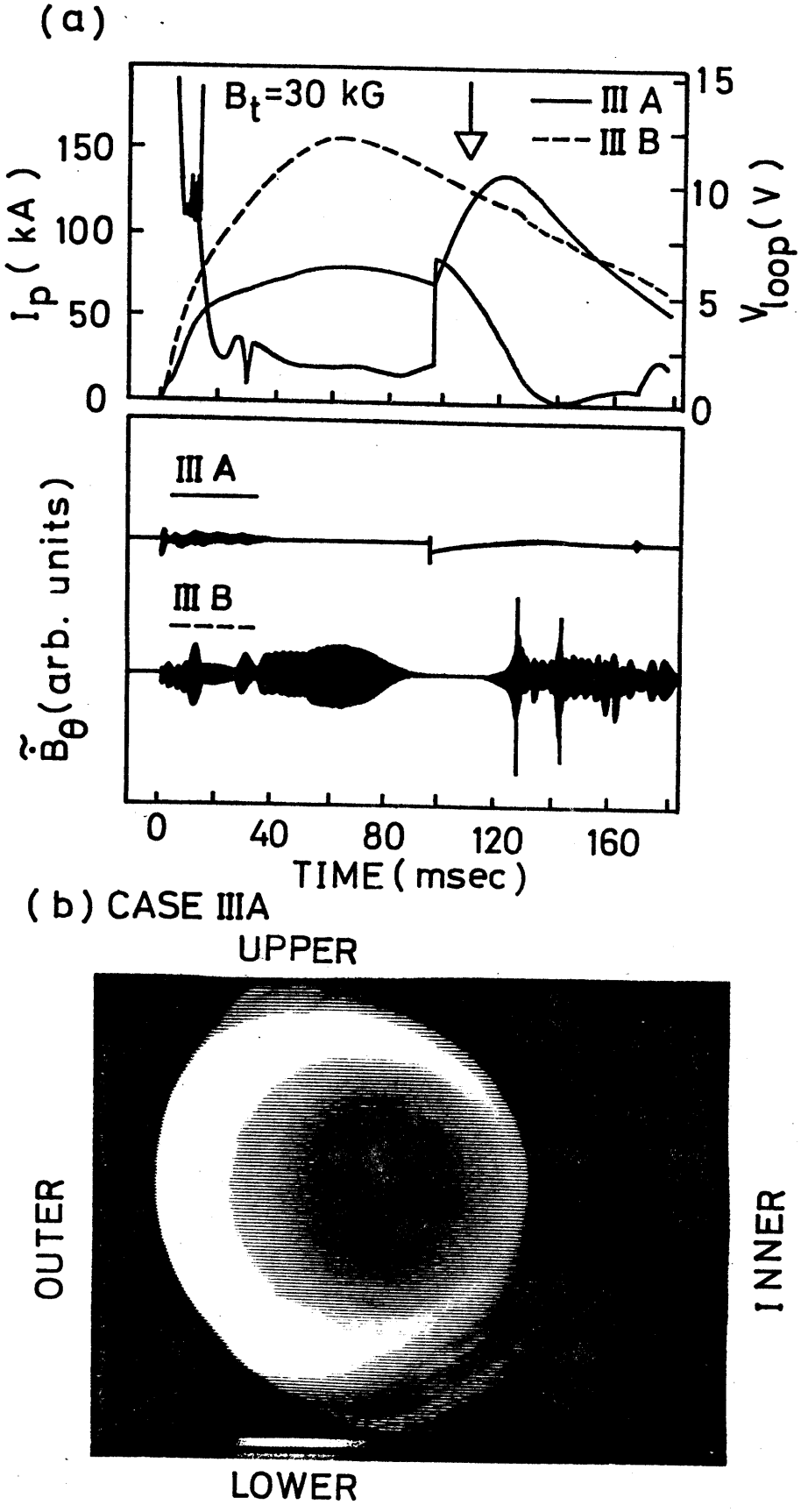
(a)
B_t=30 kG
III A
III B
I_p (kA)
V_{loop} (V)
150
100
50
0
15
10
5
0
III A
III B
$\tilde{B}_\theta$(arb. units)
0
40
80
120
160
TIME (msec)
(b) CASE IIIA
UPPER
OUTER
INNER
LOWER

Fig.16

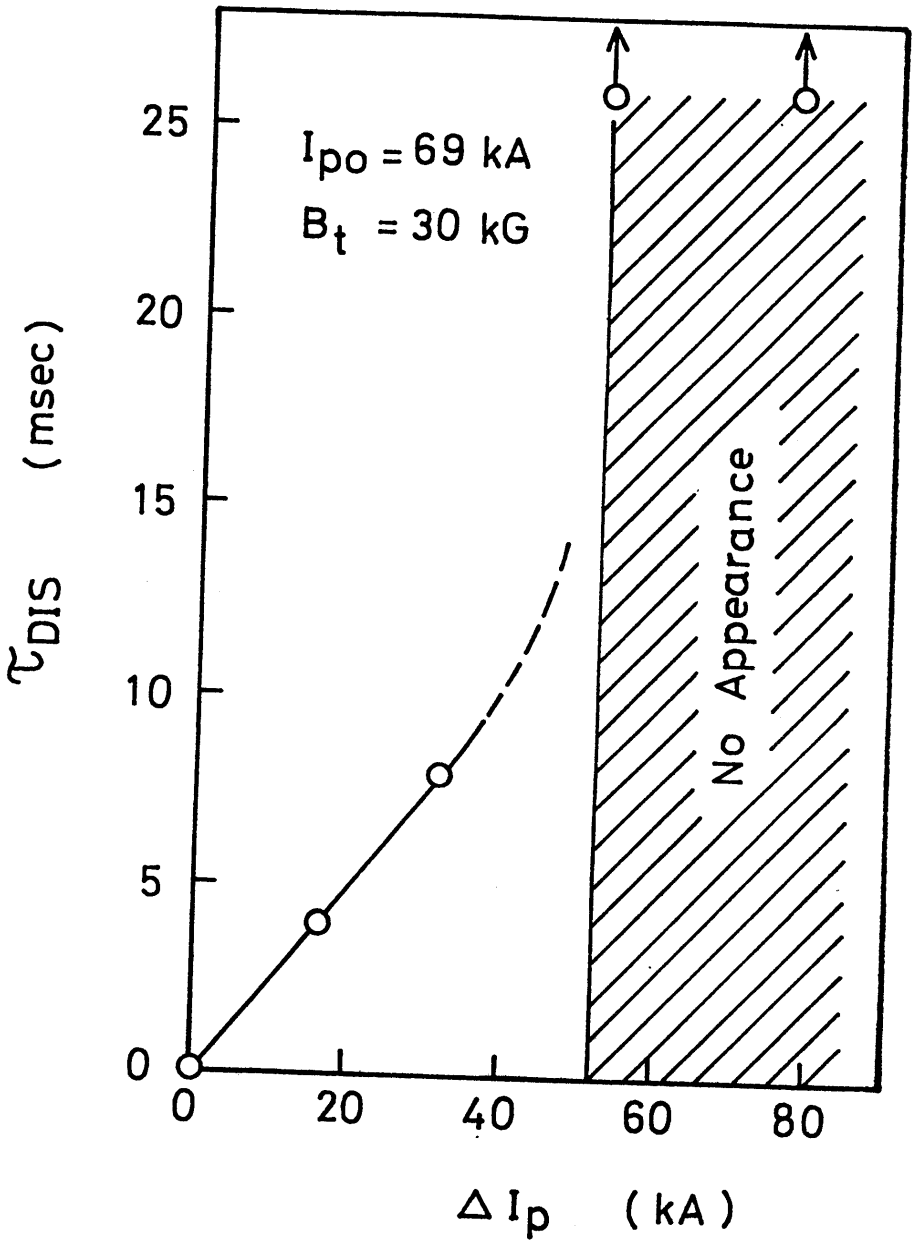
I_{po} = 69 kA
B_t = 30 kG
No Appearance
τ_{DIS} (msec)
ΔI_p (kA)
0
5
10
15
20
25
0
20
40
60
80

Fig.17

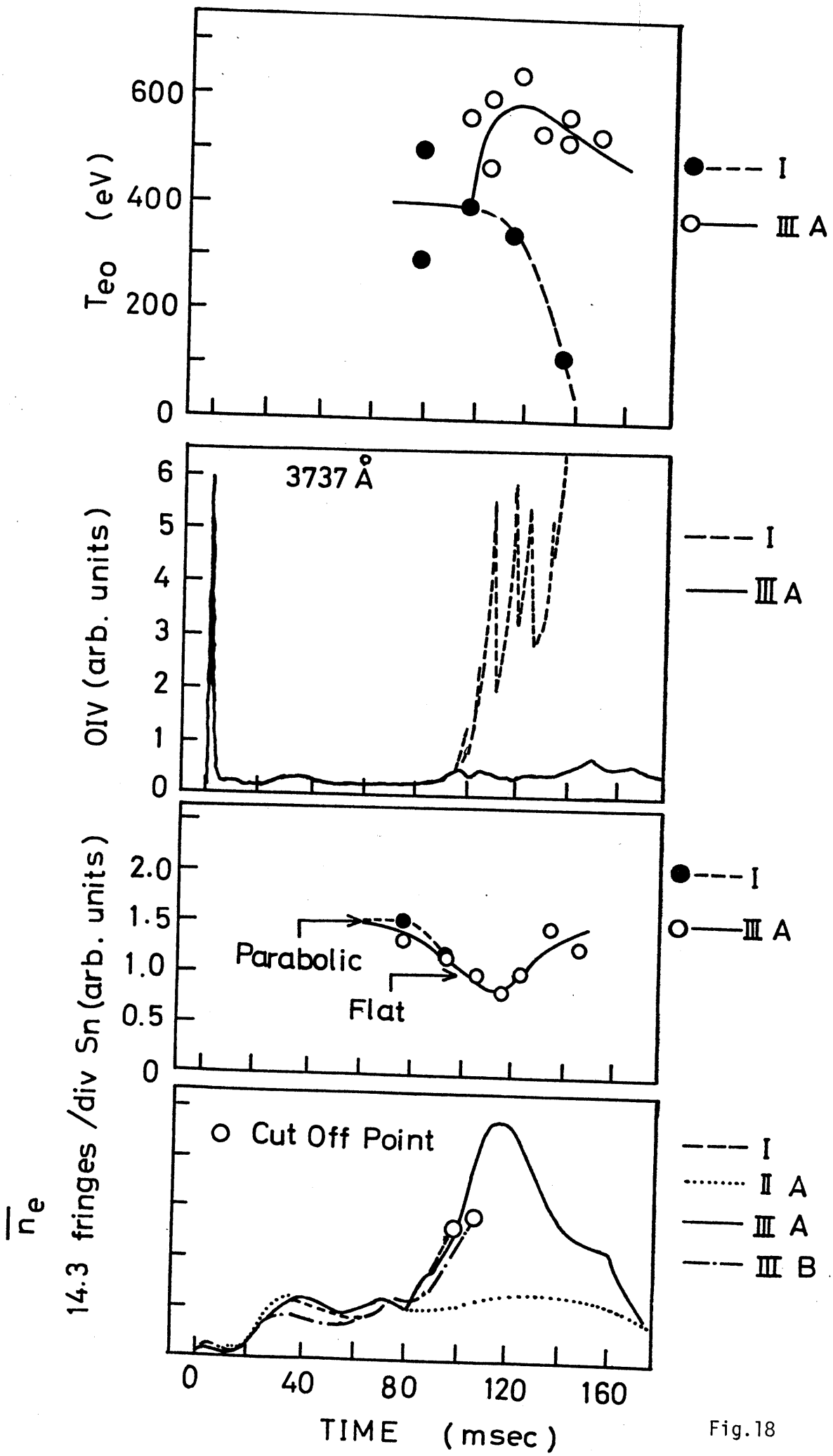
600
400
200
0
T_{eo} (eV)
I
III A
3737 Å
6
5
4
3
2
1
0
OIV (arb. units)
I
III A
2.0
1.5
1.0
0.5
0
Parabolic
Flat
I
III A
Cut Off Point
I
II A
III A
III B
0
40
80
120
160
TIME (msec)
$\overline{n}_e$
14.3 fringes /div Sn (arb. units)

Fig.18